

Characteristics and corrosion behavior of Ti–30Nb–5Sn alloys in histidine solution with various NaCl concentrations

E.P. Utomo,^{id} S. Herbirowo,^{id}* V. Puspasari and Y.N. Thaha^{id}

Research Center for Metallurgy and Materials, Indonesian Institute of Sciences, Gedung 470, 15314, South Tangerang, Banten, Indonesia

*E-mail: satr006@lipi.go.id

Abstract

The electrochemical studies of the Ti–30Nb–5Sn arc vacuum furnace's corrosion behaviour were performed in histidine solution, and the effect of NaCl addition on the corrosion behaviour of Ti–30Nb–5Sn in histidine was investigated using electrochemical impedance spectroscopy (EIS), potentiodynamic polarization, as well as Bode phase angle plot. Meanwhile, the microstructure and mechanical properties of Ti–30Nb–5Sn were examined before and after homogenization with micro-Vickers as well as optical microscopy. X-Ray Diffraction test was also conducted to characterize the phase contained before and after the homogenization of Ti–30Nb–5Sn alloys. Based on this analysis, the heat treatment at 1000°C for 5 h was discovered to increase the hardness properties of 346.7 HV and the respective beta phase transformation along the alloys' grain boundaries. Consequently, the corrosion potential in heat-treated alloys was increased by 0.14% histidine +0.12% NaCl, compared to 0.14% histidine + 3% NaCl –442.0 mV, hitting E_{corr} –385.0 mV. In addition, the highest corrosion rate was observed in the samples within 0.14% histidine + 3% NaCl of $15.53 \cdot 10^{-3}$ mmpy. Therefore, the presence of histidine contributed to a higher level of corrosion potential and the addition of NaCl into the histidine solution increased the corrosion rate of Ti–30Nb–5Sn.

Keywords: Ti–30Nb–5Sn, histidine solution, homogenization treatment, corrosion rate.

Received: February 16, 2021. Published: April 15, 2021

doi: [10.17675/2305-6894-2021-10-2-7](https://doi.org/10.17675/2305-6894-2021-10-2-7)

1. Introduction

Currently, titanium alloys are a popular choice for biomedical applications, compared to stainless steel and Cr–Mo counterpart, due to the high specific strength, modulus elasticity, durability, and biocompatibility [1]. Titanium as implant materials have a modulus elasticity of 110 GPa, and this is higher, compared to the modulus elasticity of human bones (10–30 GPa) [2], but lower than stainless steel (220 GPa) and Cr–Mo alloy (230 GPa). Therefore, titanium is superior to other representative metallic biomaterials, including stainless steel (especially SUS 316 L stainless steel) and Co–Cr–Mo alloys [3]. Generally, metallic biomaterials require a modulus elasticity value close to bone to avoid bone resorption and achieve great bone modeling [4]. The biomedical material requirements must also adapt to the human body, to avoid rejection by human body tissue. In addition, titanium biomedical alloys have low-density and excellent corrosion resistance, as well as a higher

balance between strength and ductility properties, compared to other metallic materials. Thus, titanium alloys are the most suitable for biomedical applications, compared to stainless steel and Cr–Co alloys [5].

The most popular titanium alloys are ($\alpha+\beta$) type Ti–6Al–4V, with Young's modulus properties (~ 110 GPa) close to the human bone (~ 30 GPa). Furthermore, the Al and V elements released from Ti–6Al–4V overtime are possible causes of several serious health problems, including Alzheimer's disease, neuropathy, and osteomalacia [6]. Also, the stress shielding generated from Ti–6Al–4V modulus elasticity often has a profound effect on patient health. This is due to the massive difference in elastic modulus between the implant material and the adjacent human bone [7]. The stress shielding effect possibly causes bone resorption and eventual loosening of the prosthetic device [8]. Recently, the investigation of Ti alloy for orthopedic material applications was focused on non-toxic and non-allergic titanium alloy, including metastable β Ti, for instance, Ti–Mo, Ti–Nb, and Ti–Zr [9]. However, Ti–Nb–based alloys are most suitable because of low elastic modulus, shape memory behaviour, and hyperelasticity [10]. The differences in the amount and type of alloying elements added to titanium have the ability to influence the microstructure and mechanical properties of β Ti alloys. Meanwhile, the β phase in Ti–Nb alloys has possible positive effects, including reduction in mechanical strength and elastic modulus [11]. The researcher discovered metastable β Ti alloys with 50 GPa elastic modulus, suitable for orthopedic application.

Thus, the addition of Sn elements in Ti–Nb alloys is able to reduce the excessive ω phase in Ti–Nb alloys because ω phase affects the Ti–Nb alloys' mechanical properties. In this study, Ti–30Nb–5Sn alloys were made by vacuum casting and homogenization was carried out at a temperature of 1000°C in a furnace. The microstructure and mechanical properties of Ti–30Nb–5Sn were examined, and an X-Ray Diffraction test was conducted to characterize the phase contained, before and after the homogenization treatment of Ti–30Nb–5Sn alloys. Another problem of using metallic materials in biomaterials applications is corrosion due to the implanted materials' reaction with bodily physiological fluids. Histidine is one of the biomolecules contained in the human body, and acts as a ligand or forms a film as well as metal complexes on the electrode surface, thus, reducing the rate of corrosion. In this study, the mechanism of histidine's effect on the corrosion processes of titanium was investigated in NaCl solution, and the concentration of histidine was varied to discover the effect of biomolecules materials in reducing the corrosion process of Ti–30Nb–5Sn alloys.

2. Experimental

2.1 Ti–30Nb–5Sn preparation

The synthesis of Ti–30Nb–5Sn based alloy materials focusing on the elemental composition of Nb in this study is 30% wt. Furthermore, the preparation process utilized high purity raw materials (above 99% purity) from Japan. The alloy material of 100 g total weight was

melted in the arc vacuum furnace under inert conditions, using argon gas. Meanwhile, a copper chamber holder with liquid cooling support was used as moulding to the final specimen and tungsten was used as the electrode material. The melt samples' fabrication process was carried out five times by heating until proper continuous homogeneously mixing was possible. Subsequently, the high-temperature homogenization treatment was carried out at 1000°C in a furnace, and the synthesized Ti–30Nb–5Sn sample was then cut using *Precicut*, to obtain a sample size of 10×10 mm, and subjected to a mounting process, using clear epoxy resin.

2.2 Materials characterization

The characterization tests performed include hardness test using the Shimazu Vickers at a load of 500 gf for 30 seconds, and up to 5 test location points, then the average value was selected, as well as a microstructure analysis with an optical microscope (Olympus DP12), previously used to carry out metallographic preparation and polishing to etching technique, with Kroll's reagent solution. In addition, the electrochemical measurement was carried out at the working station for potentiated polarization and these experiments were carried out in a corrosion cell with three electrodes, calomel electrode as the reference electrode and platinum wire as the counter electrode, as well as the working electrode. The experiments were conducted at neutral pH and room temperature in the histidine solution, while the potentiodynamic polarization curve was reported at a scan rate of 0.5 mV/s.

3. Results and Discussion

Table 1 shows the results of chemical analysis by the EDS instrument. The detection of material elements is performed randomly at one point in the sample. Also, evaporation of Sn is minimal during the alloy synthesis, as proven by the target composition. This shows the elemental composition before/after the homogenization, was distributed significantly.

Table 1. Chemical composition of Ti–30Nb–5Sn using Energy Dispersive Spectroscopy.

Alloy	Ti	Nb	Sn
Ti–30Nb–5Sn (before homogenization)	65.4	30.0	4.7
Ti–30Nb–5Sn (after homogenization)	66.0	29.5	4.5

Table 2. Mechanical strength of Ti–30Nb–5Sn using Hardness Vickers and Modulus.

Alloy	Hardness, HV		E, GPa	
	Before	After	Before	After
Ti–30Nb–5Sn	312.2	346.7	112.95	108.13

Table 2 shows the hardness of the Ti–30Nb–5Sn alloy in each process. The hardness and strength of as-cast increased in cases where homogenization was performed at a temperature of 1000°C (above β -transus). This is due to the emergence of the α phase after the homogenization process, followed by rapid cooling with ice water, as confirmed by XRD testing (Figure 1). The β phase has a BCC crystal structure with more slip systems, compared to the α phase, with the HCP crystal structure. The slip system is a combination of a slip plane and the slip direction, where the dislocation movement occurs. An increase in the areas allowing the dislocation movement, increase the ease of moving the dislocation, and consequently, deforming. Thus, Ti–30Nb–5Sn alloy's hardness with five times melting increased after homogenization, followed by rapid cooling with ice water. In cases where homogenization is carried out at 1000°C for 5 h, then followed by rapid cooling, the α phase is formed in addition to the β phase, as shown by the XRD results. The α phase is not evenly distributed, and forms precipitation.

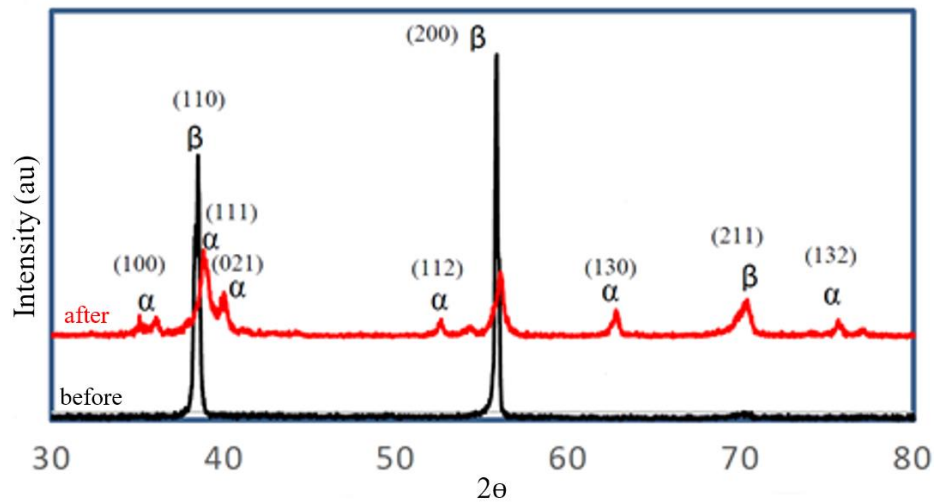


Figure 1. The XRD pattern of Ti–30Nb–5Sn alloy before and after homogenization.

Figure 1 shows the metallographic results of the homogenization process, where the equiaxed structure has a finer β phase and smaller grains, compared to the as-cast microstructure. This is because ice water is a relatively fast cooling medium, thus, the nucleation process and grain growth were not completed. Cooling water is able to change the β phase into martensite (α). Figure 2(b) shows this α phase with a lighter color, while the β phase is shown in a darker color. This is because the β phase has a lower corrosion rate, compared to the phase α , at the time of etching, a process of corroding.

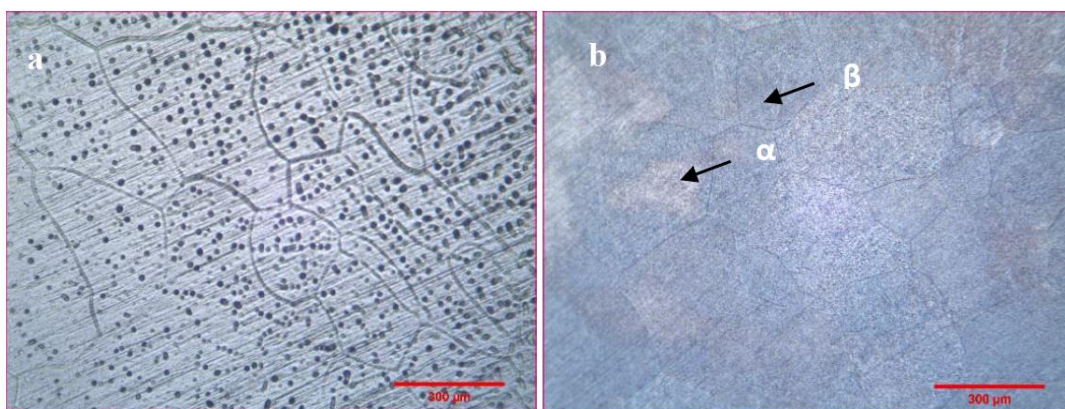


Figure 2. The microstructure of Ti–30Nb–5Sn *a)* Before and *b)* After homogenization.

Figure 2 shows the polarization curves of titanium in histidine and NaCl solution. The parameters of corrosion, corrosion potential (E_{corr}) and corrosion current density (I_{corr}) were obtained from the Tafel area. Furthermore, the corrosion current characterizes the alloy's degree of degradation, and is used to establish the alloy's corrosion rate. Various passive areas were experimental on the anodic polarization curves, where the formation of passive films arises, and the corrosion rate was determined from the corrosion current density, using the equation according to ASTM Standard G102-89.

Based on these curves, the calculated average risk for corrosion were -323 mV, -385 mV, -439 mV, -442 mV, and -384 mV for 0.14 histidine, 0.14 histidine + 0.12 NaCl, 0.14 histidine + 0.6 NaCl, 0.14 histidine + 3 NaCl, and 3 NaCl solutions, respectively. The E_{corr} values were observed to move toward the negative direction in the presence of histidine and NaCl solutions, and this is in agreement with Tafel measurements. In all tested solutions, the adjustment of the E_{corr} values were in the negative direction, the addition of NaCl led to the most pronounced shift in the solution. Furthermore, the decrease in current density is due to the formation of a protective layer with improved protective properties, and a passive region is established at a more negative potential in 3% NaCl solution, compared to the passive region obtained in the bare 0.114% histidine [12].

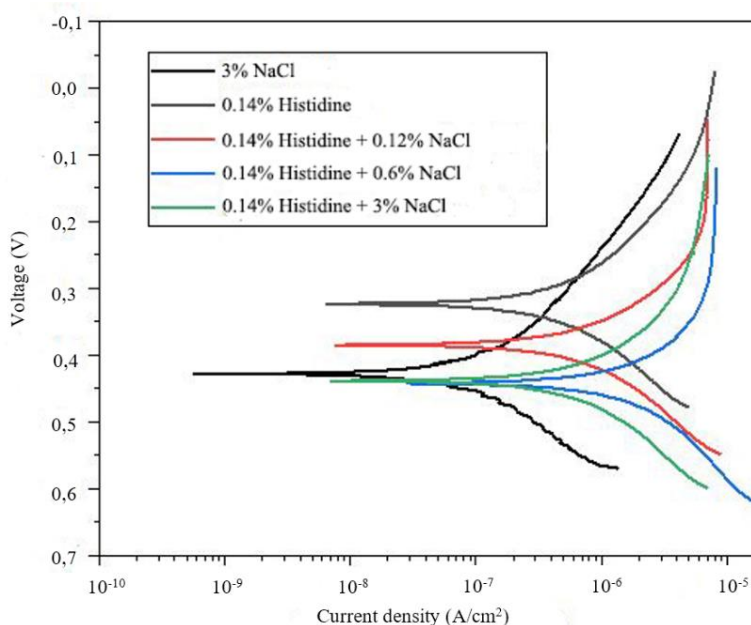
All five Ti alloys' polarization curves are V-shaped, within the range from the potential of corrosion to around -0.05 V. At approximately $4 \cdot 10^{-5}$ A/cm², the potential of sample in histidine solution begins to increase more rapidly and proceeds slowly at about -0.3 V. Meanwhile, in the NaCl solution, the rapid growth begins at around the same potential as the other four alloys. However, in all five curves, this action is the continuation of slower development, characterized by a partial steadiness of current density. This indicates the creation of a highly protective passive film in this range of potential, and is in line with the extremely low values of I_{corr} (Table 1). For the histidine and NaCl mixed solution, the current density starts to increase at approximately -0.45 V and stabilizes again at a current density of about 10^{-5} A/cm². In this case, the current density becomes stable at a slightly lower value, compared to the previous solutions, and these were able to recommend passive film breakdown, in a way comparable to pitting nucleation and re-passivation [13].

Table 3. Average values of E_{corr} and I_{corr} determined for the five Ti–30Nb–5Sn alloys from the polarization curves obtained in naturally aerated NaCl and histidine solution.

Electrolyte	E_{corr} , mV	I_{corr} , A/cm ²	Corr. rate, mmpy
0.14% histidine	–323.0	$805.0 \cdot 10^{-9}$	$11.05 \cdot 10^{-3}$
0.14% histidine+0.12% NaCl	–385.0	$1.060 \cdot 10^{-6}$	$14.54 \cdot 10^{-3}$
0.14% histidine+0,6% NaCl	–439.0	$1.130 \cdot 10^{-6}$	$15.53 \cdot 10^{-3}$
0.14% histidine+3% NaCl	–442.0	$1.260 \cdot 10^{-6}$	$17.26 \cdot 10^{-3}$
3% NaCl	–384.0	$23.30 \cdot 10^{-6}$	$3129 \cdot 10^{-3}$

Table 3 summarizes the electrochemical parameters, including the corrosion potential (E_{corr}) and corrosion current density (I_{corr}) of Ti–30Nb–5Sn alloys, in NaCl concentration and histidine solution. The I_{corr} of the alloy under varying electrolyte conditions ranged from $428.0 \cdot 10^{-9}$ A/cm² (low) to $23.30 \cdot 10^{-6}$ A/cm² (high). Subsequently, the I_{corr} value increased with an increase in NaCl added, and NaCl addition to 0.14% histidine solution can increase the corrosion rate of Ti–30Nb–5Sn (Table 3). A higher corrosion rate tends to reduce the corrosion resistance of Ti–30Nb–5Sn alloys. The lowest corrosion rate was observed in the sample in 0.14% histidine solution, indicating the highest corrosion resistance.

A prior inspection exposed a small reduction in I_{corr} , with time, pointing to the surface film's slow growth and this tends to reduce corrosion rate. Table shows all the values obtained from the various potentiodynamic polarization curves for E_{corr} and I_{corr} . However, alloys of similar composition, made by arc melting, have demonstrated similar good passivation behavior in artificial physiological solutions [14].

**Figure 3.** Potentiodynamic polarization curves for Ti–30Nb–5Sn immersed in NaCl and histidine solutions.

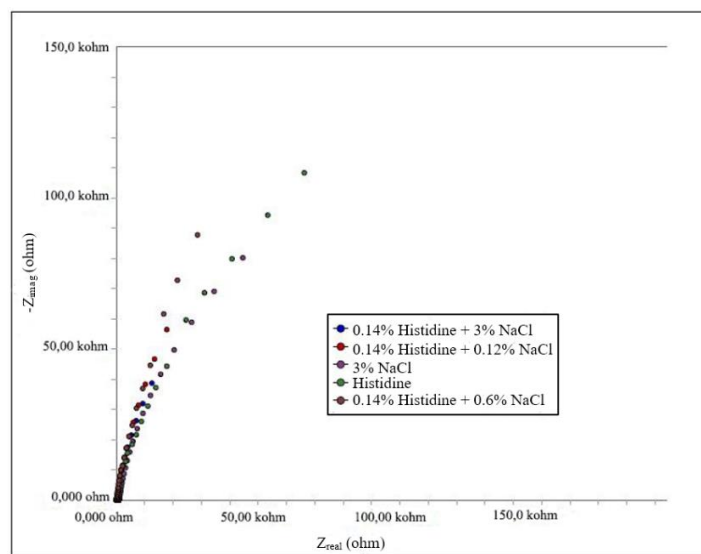


Figure 4. Nyquist plot of Ti–30Nb–5Sn in various histidine and NaCl solutions.

Figure 4 shows the results of the EIS measurement performed in various solutions, to further investigate the influence of various solutions on the corrosion behaviour of Ti–30Nb–5Sn alloys. According to Figure 4, the Nyquist plot of all experiments on Ti–30Nb–5Sn obtained from EIS measurements show an impedance of real and image results. In addition, there were some visible slopes in the curve, decreasing with increase in the addition of NaCl. The apparent capacitive arc associated with the double-layer are the passive film capacitance, and the capacitive arc radius of mixed histidine and NaCl solutions containing samples are significantly higher, compared to a single solution of histidine or NaCl. Also, the higher radii was indicated by Ti–30Nb–5Sn in 0.14% histidine +0.6% NaCl solution, however, the enhancement of NaCl percentage in mix solution of histidine and NaCl, leads to a reduction in the arc radii.

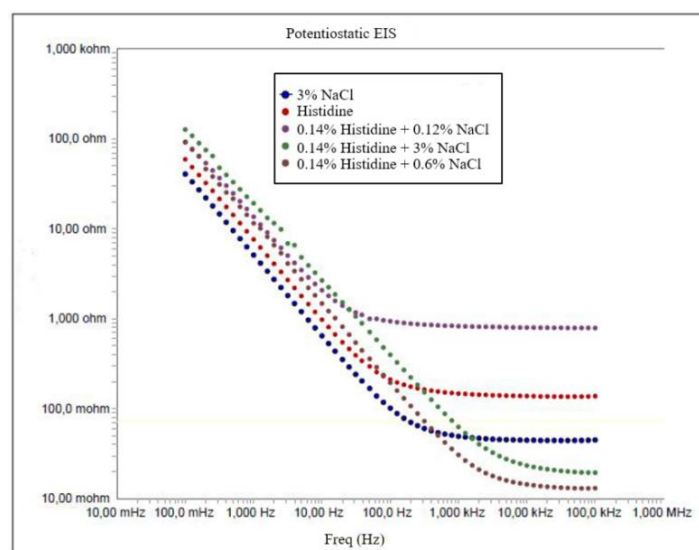


Figure 5. Z modulus of Ti–30Nb–5Sn in various histidine and NaCl solutions.

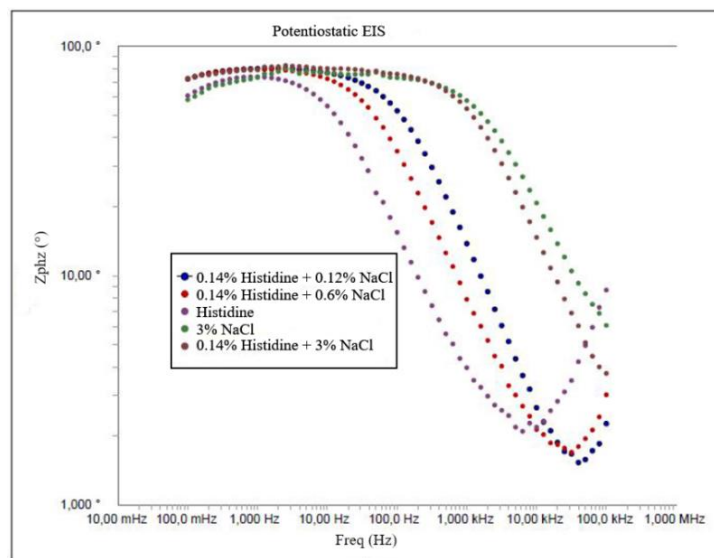


Figure 6. Bode phase angle plot of Ti–30Nb–5Sn in various histidine and NaCl solutions.

Figures 5 and 6 show the Bode plot analysis, reflecting the same tendency as Nyquist results for different samples. In addition, Figure 5 shows the Z modulus of Ti–30Nb–5Sn in various histidine and NaCl solutions. The Bode plot analysis is differentiated into two, based on frequency, and these are low frequency ($f < 10$ Hz) as well as high frequency ($f > 100$ Hz). Furthermore, the impedance value in Ti–30Nb–5Sn within low frequency showed a passive layer was formed, and a higher impedance value in low frequency, tends to increase the alloy's corrosion resistance. According to Figure 5, Ti–30Nb–5Sn alloys exhibited maximum impedance under low frequency in all variation of solutions. The highest impedance, above 100 Ohm, was obtained from Ti–30Nb–5Sn in 0.14% histidine + 3% NaCl solution, while the lowest was exhibited by Ti–30Nb–5Sn alloys in 3% NaCl.

Figure 6 shows the Bode phase angle plot of Ti–30Nb–5Sn, in various histidine and NaCl solutions. The Bode phase angle reveals a material's surface properties at high frequencies, supporting the passive layer's ability to cover. According to Figure 6, in Ti–30Nb–5Sn alloys under high-frequency, the phase angle is reduced and close to zero, however, some samples, including Ti–30Nb–5Sn alloys in 0.14% histidine + 0.12% NaCl, as well as 0.14% histidine + 0.6% NaCl and histidine, show an enhancement of the phase angle after the reduction. Furthermore, the enhancement of the Bode phase angle led to an enhancement in corrosion resistance of the Ti–30Nb–5Sn alloys. The highest maximum phase angle of Ti–30Nb–5Sn in 0.12% histidine + 0.6% NaCl is 73.04° , showing an improvement in the corrosion properties of Ti–30Nb–5Sn alloys.

4. Conclusions

- This study investigated the effect of heat treatment at 1000°C for 5 h on the mechanical, phase transformation, microstructure, and corrosion behavior of Ti–30Nb–5Sn alloys in histidine and NaCl solutions.

- The heat treatment was discovered to cause a more uniform distribution of the element composition and the respective transformation beta phase along the grain boundaries, in the Ti–30Nb–5Sn alloy.
- The effect of NaCl addition in histidine solution can increase corrosion rate and reduce the corrosion resistance of Ti–30Nb–5Sn alloys.
- The addition of 0.14% histidine +3% NaCl reduced corrosion resistance in heat-treated alloys to $17.26 \cdot 10^{-3}$ mmpy, compared to the corrosion rate of $14.54 \cdot 10^{-3}$ mmpy obtained with 0.14% histidine + 0.12% NaCl of, hitting corrosion rate of. Therefore, the addition of NaCl into histidine solution increased the corrosion rate of Ti–30Nb–5Sn, while the presence of histidine contributed to a higher level of corrosion potential.

5. Acknowledgements

The author is grateful to the Research Center for Metallurgy and Materials, Indonesian Institute of Sciences, for the provision of laboratory facilities.

References

1. J.O. Wright, N.W. Skelley, R.P. Schur, R.M. Castile, S.P. Lake and R.H. Brophy, Microstructural and Mechanical Properties of the β -Type Ti-Nb-Sn Biomedical Alloys with Low Elastic Modulus, *Metals*, 2019, **9**, no. 712, 1–16. doi: [10.3390/met9060712](https://doi.org/10.3390/met9060712)
2. M. Niinomi, Recent metallic materials for biomedical applications, *Metal. Mater. Trans. A*, 2002, **33 A**, 477–486. doi: [10.1007/s11661-002-0109-2](https://doi.org/10.1007/s11661-002-0109-2)
3. S. Guo, Q. Meng, X. Zhao, Q. Wei and H. Xu, Design and fabrication of a metastable β -type titanium alloy with ultralow elastic modulus and high strength, *Sci. Rep.*, 2015, **5**, no. 14688, 1–8. doi: [10.1038/srep14688](https://doi.org/10.1038/srep14688)
4. M. Niinomi, Y. Liu, M. Nakai, H. Liu and H. Li, Biomedical titanium alloys with Young's moduli close to that of cortical bone, *Regen. Biomater.*, 2016, **1**, 1–13. doi: [10.1093/rb/rbw016](https://doi.org/10.1093/rb/rbw016)
5. Y. Li, C. Yang, H. Zhao, S. Qu, X. Li and Y. Li, New developments of Ti-based alloys for biomedical applications, *Materials*, 2014, **7**, 1709–1800. doi: [10.3390/ma7031709](https://doi.org/10.3390/ma7031709)
6. S.M.C. van Bohemen, J. Sietsma and S. van der Zwaag, Experimental observations elucidating the mechanisms of structural bcc-hcp transformations in β -Ti alloys, *Phys. Rev. B.*, 2006, **74**, no. 13, 134114. doi: [10.1103/PhysRevB.74.134114](https://doi.org/10.1103/PhysRevB.74.134114)
7. H.N. Yu, H.C. Hsu, S.C. Wu, S.K. Hsu and W.F. Ho, Structure and mechanical properties of as-cast Ti-5Sn-xMo alloys, *Materials (Basel)*, 2017, **10**, no. 458, 1–11. doi: [10.3390/ma10050458](https://doi.org/10.3390/ma10050458)
8. M. Long and H.J. Rack, Titanium alloys in total joint replacement – a materials science perspective, *Biomaterials*, 1998, **19**, 1621–1639. doi: [10.1016/S0142-9612\(97\)00146-4](https://doi.org/10.1016/S0142-9612(97)00146-4)

9. S. Bahl, A.S. Krishnamurthy, S. Suwas and K. Chatterjee, Corrigendum to “Controlled nanoscale precipitation to enhance the mechanical and biological performances of a metastable β Ti-Nb-Sn alloy for orthopedic applications”, *Mater. Des.*, 2017, **130**, no. 349, 226–237. doi: [10.1016/j.matdes.2017.05.072](https://doi.org/10.1016/j.matdes.2017.05.072)
10. B.L. Wang, Y.F. Zheng and L.C. Zhao, Effects of Sn content on the microstructure, phase constitution and shape memory effect of Ti-Nb-Sn alloys, *Mater. Sci. Eng. A*, 2008, **486**, 146–151. doi: [10.1016/j.msea.2007.08.073](https://doi.org/10.1016/j.msea.2007.08.073)
11. F.F. Cardoso, P.L. Ferrandini, E.S.N. Lopes, A. Cremasco and R. Caram, Ti-Mo alloys employed as biomaterials: Effects of composition and aging heat treatment on microstructure and mechanical behavior, *J. Mech. Behav. Biomed. Mater.*, 2014, **32**, 31–38. doi: [10.1016/j.jmbbm.2013.11.021](https://doi.org/10.1016/j.jmbbm.2013.11.021)
12. M.B. Radovanović, Ž.Z. Tasić, A.T. Simonović, M.B. Petrović Mihajlović and M.M. Antonijević, Corrosion Behavior of Titanium in Simulated Body Solutions with the Addition of Biomolecules, *ACS Omega*, 2020, **5**, 12768–12776. doi: [10.1021/acsomega.0c00390](https://doi.org/10.1021/acsomega.0c00390)
13. S.L. De Assis, S. Wolyneć and I. Costa, Corrosion characterization of titanium alloys by electrochemical techniques, *Electrochim. Acta*, 2006, **51**, no. 8–9, 1815–1819. doi: [10.1016/j.electacta.2005.02.121](https://doi.org/10.1016/j.electacta.2005.02.121)
14. D.S.M. Vishnu, J. Sure, R.V. Kumar and C. Schwandt, Phase composition, microstructure, corrosion resistance and mechanical properties of molten salt electrochemically synthesised TiNbSn biomedical alloys, *Mater. Trans.*, 2019, **60**, no. 3, 422–428. doi: [10.2320/matertrans.MA201810](https://doi.org/10.2320/matertrans.MA201810)

